Faraday Discussions

Cite this: DOI: 10.1039/d5fd00166h

PAPER

Surface vibrations, polaritons and their coupling to a 2D electron gas: interface-bound vibrations at the $SrTiO_3$(001) surface

Hannes Herrmann, Anne Oelschläger and Wolf Widdra *

Received 14th December 2025, Accepted 9th February 2026
DOI: 10.1039/d5fd00166h

The low-energy excitations of $SrTiO_3$, a large-bandgap oxide perovskite, are dominated by phonons and phonon polaritons. At the surface they couple to dipole-active surface phonon polaritons that are bound to the $SrTiO_3$–vacuum interface. These excitations can be addressed by surface vibrational spectroscopy techniques such as, *e.g.*, high resolution electron energy loss spectroscopy (HREELS). The HREELS experiments identify all $SrTiO_3$(001) dipole-active surface excitations, including their specific line shape and their electron–phonon coupling to a two-dimensional electron gas (2DEG). The latter is prepared by a surface reduction *via* annealing under ultrahigh-vacuum conditions. With formation of the 2DEG, the discrete surface phonon polaritons couple to the electron–hole pair continuum as is witnessed by a substantial line broadening and asymmetric Fano-like line shape.

Introduction

The cubic or pseudocubic perovskite oxides with the general formula ABO_3 exhibit a variety of interesting physical properties, such as high-temperature superconductivity, colossal magnetoresistance, ferroelectricity, multiferroicity, and catalytic activity.[1–5] Many of these properties are closely related to the lattice dynamics and the coupling between lattice vibrations (phonons) and charge carriers.[4,5] In particular, the interaction between electrons and polar optical phonons plays a crucial role in determining the electronic transport properties and the formation of exotic states such as polarons.[6]

In the cubic phase as found for $SrTiO_3$ at room temperature, the lattice dynamics are characterized by three degenerate dipole-active optical phonon eigenmodes at the Γ-point (all of symmetry F_{1u}) which are traditionally classified as Last,[7] Slater,[8] and Axe[9] modes as shown in Fig. 1.

The Last[7] mode corresponds to the movement of the A-site cations (Sr^{2+} in $SrTiO_3$) against the rigid TiO_6 octahedra framework (Fig. 1(a)), the Slater[8] mode

Institute of Physics, Martin-Luther-Universität Halle-Wittenberg, von-Danckelmann-Platz 3, 06198 Halle, Germany. E-mail: wolf.widdra@physik.uni-halle.de

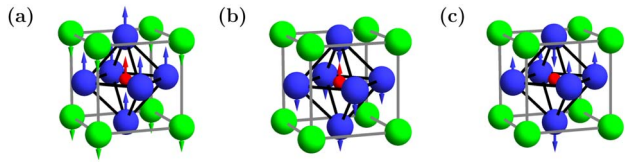

Fig. 1 Eigenmodes of the three dipole-active cubic perovskite phonons with F_{1u} symmetry, known as Last[7] (a), Slater[8] (b), and Axe[9] (c) modes.

are mutual vibrations of the Ti cations against the oxygen octahedra (Fig. 1(b)), and the higher frequency Axe[9] mode involves the deformation of the oxygen octahedra (Fig. 1(c)). Note that the softening of the Slater mode at low temperatures is responsible for the incipient ferroelectric behavior of $SrTiO_3$.[10] The dielectric function $\varepsilon(\omega)$ of $SrTiO_3$ at the Γ point can be well described by these three oscillators using a generalized four-parameter oscillator model[11–14] that takes into account different damping of transverse optical (TO) and longitudinal optical (LO) modes:

$$\varepsilon(\omega) = \varepsilon_\infty \prod_{j=1}^{3} \frac{\omega_{\mathrm{LO}_j}{}^2 - \omega^2 + \mathrm{i}\omega\gamma_{\mathrm{LO}_j}}{\omega_{\mathrm{TO}_j}{}^2 - \omega^2 + \mathrm{i}\omega\gamma_{\mathrm{TO}_j}}. \quad (1)$$

where ε_∞ is the high-frequency dielectric constant. ω_{TO_j} and ω_{LO_j} are the frequencies of the j-th transverse and longitudinal optical phonon modes, respectively, while γ_{TO_j} and γ_{LO_j} are their corresponding damping constants. The dielectric function captures the frequency-dependent response of the material to an external electric field, which is essential for understanding the behavior of polaritons and their interaction with charge carriers. To probe the dielectric response, light absorption and energy loss spectroscopy techniques are powerful tools as they are sensitive to the energy loss function $L(\omega)$ given by:

$$L_{\mathrm{bulk}}(\omega) = -\mathrm{Im}\left(\frac{1}{\varepsilon(\omega)}\right). \quad (2)$$

It describes the energy loss of fast electrons as they interact with the material, providing insights into the vibrational modes and their coupling to electronic excitations. Peaks in the energy loss function correspond to the frequencies of the optical phonon modes, allowing for their identification and characterization.

At the surface of $SrTiO_3(001)$, the material–vacuum interface leads to the emergence of surface phonon polaritons (SPhP), which are electromagnetic modes coupled to the lattice vibrations. These modes are confined to the interface between $SrTiO_3$ and vacuum, exhibiting unique dispersion relations and field distributions compared to bulk phonons. The SPhPs can be probed using surface-sensitive techniques such as high-resolution electron energy loss spectroscopy (HREELS), which allows for the investigation of their dispersion and their coupling to electronic states. In this study, we employ HREELS to investigate the SPhPs of $SrTiO_3(001)$ and their interactions with a two-dimensional electron gas (2DEG) formed at the surface of $SrTiO_3$. The 2DEG can be generated by annealing the $SrTiO_3$ surface under ultrahigh-vacuum conditions or by UV radiation.[5,15–18] The presence of free charge carriers in the 2DEG is expected to lead to significant modifications of the surface phonon polariton spectra, including line broadening

and asymmetric Fano-like line shapes due to a strong coupling between the phonons and the 2D electron–hole pair continuum.

At the surface of a material with a bulk dielectric response $\varepsilon(\omega)$, the energy loss function is quantitatively described by:

$$L_{\mathrm{surf}}(\omega) = -\mathrm{Im}\left(\frac{1}{\varepsilon(\omega)+1}\right). \tag{3}$$

This expression accounts for the boundary conditions at the interface, where the dielectric function of the material interacts with that of the vacuum. The surface energy loss function captures the unique vibrational properties of the interface, including the presence of SPhPs, which can exhibit distinct dispersion relations and coupling behaviors compared to bulk phonons. The relation between the bulk and surface loss functions as well as the real and imaginary parts of the dielectric function is illustrated later in Fig. 2 and 3 for $SrTiO_3(001)$ together with the HREELS spectrum.

For metallic systems which include also 2DEGs at the surface of perovskite oxides, the free charge carriers contribute an additional term to the dielectric function, typically described by the Drude model. The dielectric response in the presence of both the phonons and the free charge carriers, is given with the additional Drude contribution to eqn (1):

$$\varepsilon(\omega) = \varepsilon_\infty \prod_{j=1}^{3} \frac{{\omega_{\mathrm{LO}_j}}^2 - \omega^2 + \mathrm{i}\omega\gamma_{\mathrm{LO}_j}}{{\omega_{\mathrm{TO}_j}}^2 - \omega^2 + \mathrm{i}\omega\gamma_{\mathrm{TO}_j}} - \varepsilon_\infty \frac{{\omega_{\mathrm{p}}}^2}{\omega^2 + i\omega\gamma_{\mathrm{p}}}. \tag{4}$$

where ω_{p} is the plasma frequency of the free carriers and γ_{p} is the Drude damping constant. This term accounts for the collective oscillations of the conduction electrons and leads to screening of the phonon modes. In the presence of a 2DEG at the surface, the coupling between surface phonon polaritons and the electronic continuum modifies the energy loss spectra, resulting in broadened and asymmetric features. The interplay between the lattice and electronic degrees of freedom is crucial for understanding the vibrational and electronic properties of oxide interfaces and their potential applications in oxide electronics, *e.g.* for a large spin-to-charge conversion effect in an interface-engineered $SrTiO_3(001)$ with a two-dimensional electron gas.[17]

Methods

The experiments were performed in an ultra-high vacuum (UHV) chamber equipped with facilities for low energy electron diffraction (LEED), X-ray photoelectron spectroscopy (XPS) and high-resolution electron energy loss spectroscopy (HREELS). The HREEL spectrometer (Delta 05, Specs, Berlin) can be operated with a monochromized electron beam with a kinetic energy between 1 and 255 eV with a total energy resolution of 1 meV for kinetic energies below 16 eV as described elsewhere.[19–23] However, all spectra shown here were recorded with a primary energy of 4 eV and an energy resolution below 2 meV in specular scattering geometry.

$SrTiO_3(001)$ single crystal substrates (CrysTec, Berlin) with 0.05% Nb doping were wet chemically etched using a buffered HF solution to obtain a TiO_2-terminated surface.[24] After introduction into the UHV chamber, the samples were

mildly annealed to 500 K to remove adsorbates. The formation of a 2DEG at the $SrTiO_3(001)$ surface was achieved here by annealing the samples to higher temperatures under UHV conditions ($p < 10^{-9}$ mbar), which results in oxygen vacancies and Ti^{3+} ions at the surface as will be discussed in Fig. 4. Alternatively, the evaporation of ultrathin layers of a reactive metal on top of $SrTiO_3(001)$ can also lead to the formation of a 2DEG at the interface due to the formation of oxygen vacancies in the surface layer of $SrTiO_3$.[15–17]

Results and discussion

The HREEL spectrum of the pristine $SrTiO_3(001)$ surface is shown as the black line in Fig. 2 together with the corresponding surface loss functions (blue line, upshifted by 200 000 counts s^{-1}). The HREEL spectrum exhibits three distinct loss features at 168, 465, and 741 cm^{-1} that can be assigned to the three surface phonon polaritons S1, S2, and S3, respectively. All other losses correspond to combinations of S1, S2 and S3. *E.g.*, the losses at 932, 1210, and 1487 cm^{-1} are sequential excitations S2 + S2, S2 + S3, and S3 + S3, respectively. The weak feature at 276 cm^{-1} corresponds to excitation of the S3 and deexcitation of the S2 mode: S3 − S2. The latter process is possible due to the thermal population of S2 at room temperature, whereas it is suppressed at low temperatures (not shown here). The assignments of the surface phonon polaritons S1, S2, and S3 to the corresponding bulk phonon modes TO1, TO2, and TO3 are summarized in Table 1.

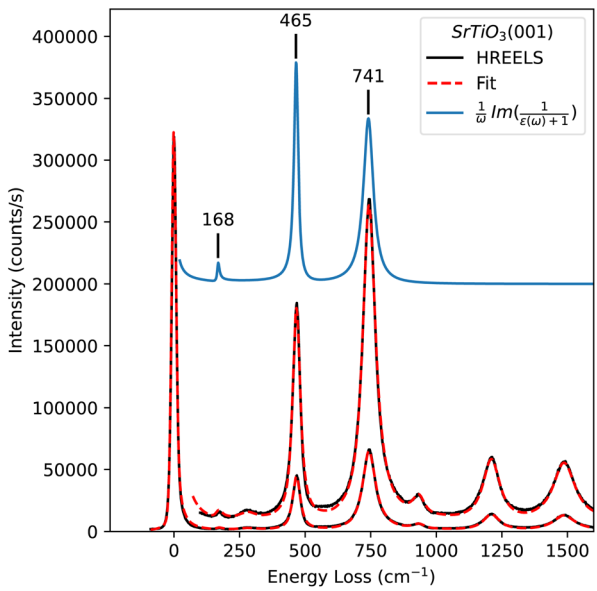

Fig. 2 HREELS spectrum of the pristine $SrTiO_3(001)$ surface (black line). The loss region is amplified by a factor of 5. Fitting by a generalized oscillator model as given in eqn (1) is shown as red dashed line. The calculated surface loss function (blue line, upshifted for clarity) as obtained from fitting the HREELS data. The three surface phonon polaritons S1, S2, and S3 are indicated.

Table 1 Phonon parameters derived from the HREELS spectrum of $SrTiO_3$(001) shown in Fig. 2. The parameters are the longitudinal optical phonon frequencies ω_{LO_j}, the transverse optical phonon frequencies ω_{TO_j}, and the damping constants γ_{LO_j} and γ_{TO_j} for $j = 1, 2, 3$. All values are given in cm^{-1}

Mode	ω_{S_j}	ω_{TO_j}	γ_{TO_j}	ω_{LO_j}	γ_{LO_j}
1	168	110.2	9.2	168.0	10.0
2	465	171.1	13.1	476.0	18.7
3	741	531.4	18.7	835.9	57.3

The complex dielectric function as reported in eqn (1) is fully determined by the parameters in Table 1 and leads to the surface loss function (blue line) shown in Fig. 2. The corresponding calculated HREELS spectrum is shown by the red dashed line in Fig. 2, which takes into account the Bose–Einstein statistics of multiple excitations, the electron kinetic energy, the scattering geometry as well as the instrumental energy broadening as determined by the zero-loss elastic peak. The calculated HREELS spectrum reproduces very well the experimental data, including all line shapes and all multiple excitations.

To achieve this good agreement, we have varied the phonon frequencies as well as the damping parameters and calculated iteratively the corresponding HREELS spectra according to the procedure of Lambin[25] *via* the surface loss function L_{surf} and a fitting of the elastic peak (zero energy loss peak). We started with literature values of the bulk phonon frequencies and determined all phonon frequencies and their damping constants by fitting the experimental HREELS data. Whereas the LO phonon frequencies are closely related to the close-lying phonon polariton peaks in the surface loss spectrum, the sensitivity of the fit to the TO phonon frequencies is lower. The fitted bulk phonon frequencies from the surface-sensitive HREELS data are in good agreement with previous reports based on bulk-sensitive techniques such as, *e.g.*, infrared spectroscopy of similarly doped samples.[26] Note that the slight differences in the phonon frequencies can be attributed to the different doping levels as well as to surface effects that may lead to small shifts of the phonon frequencies at the surface compared to the bulk. The resulting bulk dielectric function is shown in Fig. 3. The real part of the dielectric function crosses the value of -1 at frequencies of 460 and 745 cm^{-1} which are in excellent agreement with the experimentally observed surface phonon polariton frequencies S2 and S3. The characters of the three phonon modes are schematically illustrated in Fig. 1.

HREEL spectra recorded after annealing the $SrTiO_3$(001) surface to higher temperatures under UHV conditions are shown in Fig. 4. For annealing temperatures between 670 and 870 K, the loss spectra show hardly any change. A detailed comparison shows only a slight increase in the linewidths of the surface phonon polaritons S2 and S3 upon annealing to 970 K. However, upon annealing to 1070 K, we observe a strong asymmetric broadening of the surface phonon polaritons S2 and S3 as well as substantial decrease of both peak intensities. The pronounced asymmetric line shapes are characteristic for Fano resonances, which arise from the interference between discrete phonon states and a continuum of electronic excitations. The presence of a 2DEG at the surface, induced by oxygen vacancies created during annealing, provides the necessary

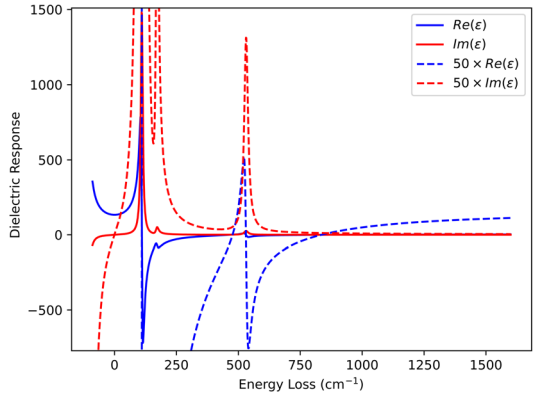

Fig. 3 Real and imaginary parts of the dielectric function $\varepsilon(\omega)$ of $SrTiO_3$(001) as obtained from fitting the HREELS data in Fig. 1.

electronic continuum for this coupling. Note that molecular oxygen adsorption will quench the 2DEG completely (not shown here) and restores a spectral response with symmetric line shapes as shown in Fig. 2 and in the top spectrum of Fig. 4.

Due to the free surface charge carriers, an additional Drude term contributes to the dielectric function as described in eqn (4). The modified dielectric function leads to a screening of the phonon modes and their coupling to the electron–hole pair continuum. This interaction results in the observed line broadening and asymmetric Fano-like line shapes in the HREELS spectra. The interplay between

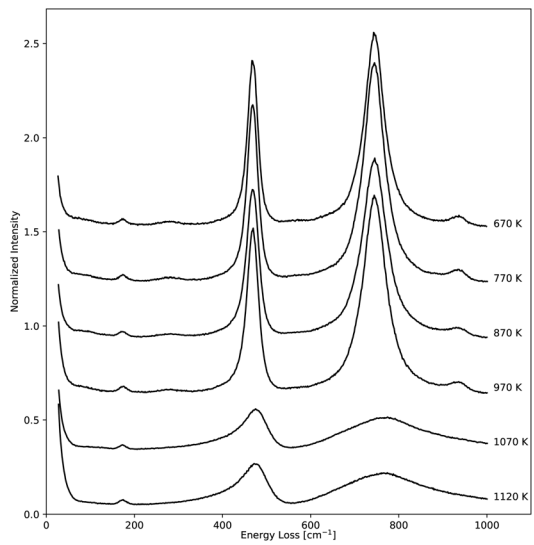

Fig. 4 HREELS spectra of $SrTiO_3$(001) after annealing to different temperatures in UHV as indicated on the right side. Upon annealing to temperatures above 970 K, the formation of a 2DEG at the surface leads to pronounced asymmetric Fano-like line shapes of the surface phonon polaritons S2 and S3.

the lattice vibrations and the electronic states at the surface is crucial for understanding the vibrational and electronic properties of oxide interfaces and their potential applications in oxide electronics, as it might lead at the surface to new quasiparticles with modified properties. From a methodological standpoint, these experiments establish the capability for high-quality *in situ* UHV characterization of a surface-bound 2DEG without requiring the fabrication of contacts on the sample.

To analyze the coupling between the surface phonon polaritons and free charge carriers, we calculate the surface phonon polariton spectra using the combined dielectric function of eqn (4) which includes the Drude term. In the absence of phonons, the Drude response alone leads to a surface-bound mode, the surface plasmon polariton, with a surface loss energy given by:

$$\omega_{SP} = \omega_p \sqrt{\frac{\varepsilon_\infty}{\varepsilon_\infty + 1}}. \tag{5}$$

Here, ω_p is the plasma frequency of the free carriers and ε_∞ is the high-frequency dielectric constant. The surface plasmon polariton frequency ω_{SP} depends, as the plasma frequency itself, linearly on the square root of the carrier concentration and the effective band mass of the charge carriers.

When phonons are included in the dielectric function, the surface phonon polaritons and the surface plasmon polariton couple to new hybrid modes as is schematically indicated in Fig. 5 for the case of one phonon and a plasmon with different plasma frequencies ω_p. The surface loss functions according to the dielectric function in eqn (1) in the presence of the additional Drude response of eqn (4) leads to two surface loss peaks. Their loss energies are depicted in Fig. 5. In the absence of a Drude response, $\omega_p = 0$, there is only one peak at the surface

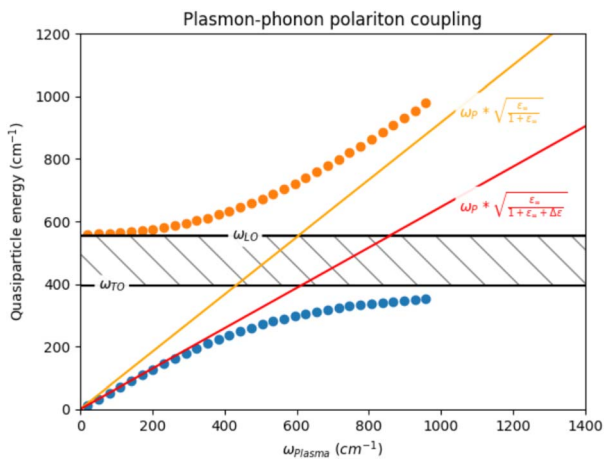

Fig. 5 Energies of the surface loss peaks as a function of the plasma frequency ω_p of the Drude response. The blue and orange circles indicate the two surface loss peaks that arise from coupling of both modes, the surface plasmon polariton and the surface phonon polariton. The hatched region between $\omega_{TO} = 393.7$ cm^{-1} and $\omega_{LO} = 584.7$ cm^{-1} corresponds to the bulk Reststrahlen band. We note an avoided crossing behavior between the two coupled modes.

phonon polariton frequency ω_S, just below the frequency of the LO bulk phonon ω_{LO}. With increasing plasma frequency ω_p, initially the surface plasmon polariton develops linearly with ω_p (blue circles). For larger ω_p, this mode levels off just below the TO bulk phonon frequency ω_{TO}. The mode which corresponds initially at $\omega_p = 0$ to the surface phonon polariton (orange circles) increases its frequency with increasing ω_p. Its character changes from phonon-like to plasmon-like with increasing ω_p. For large ω_p, this mode approaches the surface plasmon polariton frequency again with the typical linear dependence on ω_p. Note that the initial frequency shift of the surface plasmon polariton, that follows the red line, is proportional to $\omega_p\sqrt{\frac{\varepsilon_\infty}{1+\varepsilon_\infty+\Delta\varepsilon}}$, where $\Delta\varepsilon$ is the contribution of the phonon mode to the dielectric function at the surface phonon polariton frequency. In other words, the surface plasmon polariton is screened additionally by the phonon mode as long as its frequency is below the phonon mode. However, the upshifting mode never enters the Reststrahlen band between ω_{TO} and ω_{LO} due to the strong coupling between both modes. Substantially above the Reststrahlen band, the surface plasmon polariton frequency scales again linearly with ω_p without influence of the phonon mode. In general, the coupling between surface phonon polariton and the surface plasmon polariton can be understood as an avoided crossing behavior as is typical for coupled oscillators.

In Fig. 6, we show the calculated surface loss peak energies in the presence of two surface phonon polaritons and a surface plasmon polariton. Here, three surface loss peaks arise from the coupling of three modes. The avoided crossing behavior is again evident, where the two upshifting modes never enter the

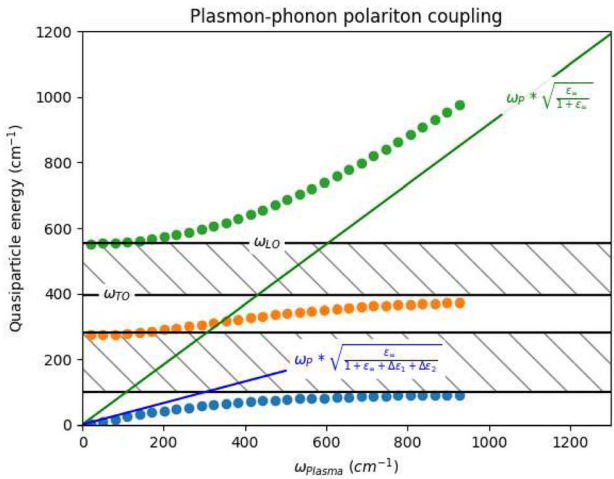

Fig. 6 Energies of the surface loss peaks as a function of the plasma frequency ω_p of the Drude response in the presence of two surface phonon polaritons. The blue, orange, and green circles indicate the three surface loss peaks that arise from coupling between the surface plasmon polariton and the two surface phonon polaritons. The hashed regions between $\omega_{TO} = 100$ cm^{-1} and $\omega_{LO} = 280$ cm^{-1} and between $\omega_{TO} = 393.7$ cm^{-1} and $\omega_{LO} = 584.7$ cm^{-1} correspond to the two Reststrahlen band. We note again the avoided crossing behavior between the three coupled modes, where the upshifting modes never enter the Reststrahlen bands.

respective Reststrahlen bands (hatched areas). Therefore, the upper bound of the lower phonon mode is limited to the TO frequency of the upper phonon mode. The initial frequency shift of the surface plasmon polariton (blue circles for small ω_p) follows the linear blue line, which is proportional to $\omega_p\sqrt{\frac{\varepsilon_\infty}{1+\varepsilon_\infty+\Delta\varepsilon_1+\Delta\varepsilon_2}}$, where $\Delta\varepsilon_j$ are the contributions of both phonon modes to the dielectric function. However, at large ω_p, the surface plasmon polariton frequency scales again linearly with ω_p without influence of the phonon modes. The strong upshift might be partially suppressed by a strongly overdamped ($\gamma_p > \omega_p$) surface plasmon polariton as is often observed in bad metals or low-mobility semiconductors.[27,28] In the latter case the peaks broaden substantially. The intensities of the three surface losses as a function of the plasma frequency ω_p are shown in Fig. 7 as blue, orange, and green solid circles according to the colors in Fig. 6. The intensity of the lowest loss peak (blue circles) is initially strongly increasing with increasing ω_p due to its plasmon character and the growing plasmon oscillator strength. At intermediate plasma frequencies, the increasing intensity shifts over to the high frequency loss peak (green circles). Finally, it leads to a decrease in the intensities of all phonon-like losses for large ω_p due to screening of the optical phonon modes by the free charge carriers.

Based on these general considerations, we can now analyze the HREELS spectrum of $SrTiO_3$(001) after annealing to 1070 K and formation of the 2DEG as shown in Fig. 4 (lower two traces). The pronounced asymmetric line shapes skew the loss peaks of the surface phonon polaritons S2 and S3 to lower and higher energies, respectively, as compared to the pristine surface (Fig. 2). In comparison with the schematic discussion above for Fig. 6 and 7, we have to take into account that the Drude response is often overdamped ($\gamma_p > \omega_p$) in oxide materials with low

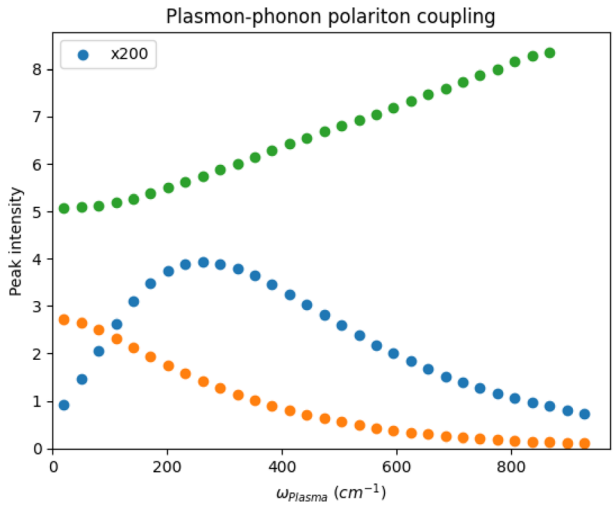

Fig. 7 Peak intensities of the surface losses as a function of the plasma frequency ω_p of the Drude response in the presence of two surface phonon polaritons. The blue, orange, and green circles indicate the three surface loss peaks as in Fig. 6 that arise from coupling between the surface plasmon polariton and the two surface phonon polaritons. The intensity of the lowest loss (blue circles) is amplified by a factor of 200.

charge carrier mobilities.[27,28] In addition, the dielectric response in the top surface layer differs from the bulk response due to the additional presence of the 2DEG that is confined to a few nanometers at the surface.[29] Therefore, we model the dielectric response of the sample by considering a multilayer structure with a surface $SrTiO_3(001)$ layer with the Drude response and a thickness of 5 nm, on top a second layer of $SrTiO_3$ without Drude contribution. The phonon properties in both areas are taken to be identical as derived above (Fig. 2) in the absence of a Drude response. For the multilayer, the HREELS spectrum is determined based on the effective dielectric response as described elsewhere.[25,30]

The calculated HREELS spectra for different plasma frequencies ω_p of the Drude response in the surface layer are shown in Fig. 8. The top spectrum is the calculated HREELS spectrum of the bare $SrTiO_3(001)$ surface without Drude response as already shown in Fig. 2 as fit to the experimental data. The subsequent spectra show the calculated HREELS spectra with increasing plasma frequencies ω_p from 250 to 1000 cm^{-1} (from second top to bottom). The Drude damping constant is chosen as $\gamma_p = 1.5 \times \omega_p$ in all cases to simulate an

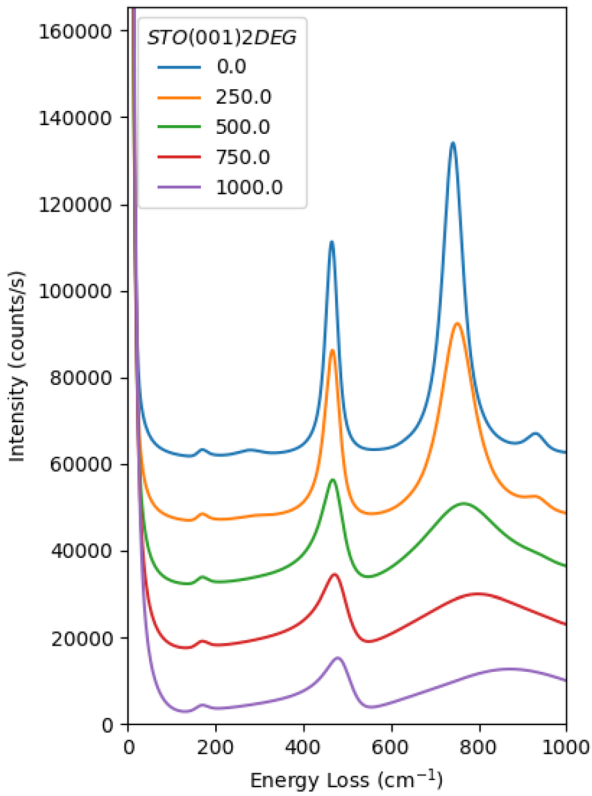

Fig. 8 Calculated HREELS spectrum of the bare $SrTiO_3(001)$ surface (top blue line) based on the parametrization according to eqn (1) and Table 1. Calculated HREELS spectra with addition of 2D electron gases (thickness 5 nm) at the surface described by an additional Drude term in the dielectric function. The free charge carrier concentration is given *via* the plasma frequency ω_p from 0, 250, 500, 750, to 1000 cm^{-1} (from top to bottom). The plasma oscillations are in all cases overdamped: $\gamma_p = 1.5 \times \omega_p$.

overdamped plasmon response. The latter leads to a substantial broadening of the surface plasmon polariton and therefore also for the coupled S3 mode. With increasing plasma frequency ω_p, the surface modes S2 and S3 shift to slightly higher energies. Both peak intensities are reduced and the peak shapes broaden substantially due to their coupling to the electronic continuum. The line shapes become asymmetric due to interference effects between the discrete phonon states and the electronic continuum. These general trends are in good agreement with the experimental observations after annealing to 1070 K as shown in Fig. 4.

A best fit to the experimental HREELS spectrum after annealing to 1070 K is shown in Fig. 9 together with experimental data on a wider energy scale. The fit (red dashed line) is obtained for a plasma frequency of about $\omega_p = 950$ cm^{-1} and a Drude damping constant of $\gamma_p = 1100$ cm^{-1}. The calculated HREELS spectrum reproduces the experimental data, including the asymmetric line shapes of the surface phonon polaritons S2 and S3 as well as their substantial broadening and intensity reduction. The blue line in Fig. 9 shows the same fit, where the Drude response is set afterwards to zero for comparison. The plasma frequency $\omega_p =$ 950 cm^{-1} corresponds to carrier concentrations of about $n_s = (1\ldots10) \times 10^{19}$ cm^{-3} depending on the effective mass of about $m^* = 0.7m_e$ as reported previously for in-plane response of 2DEGs at $SrTiO_3$(001) surfaces.[15] It corresponds to free charge carriers of only a fraction of an electron per unit cell area in the surface layer of $SrTiO_3$(001) – (1 × 1).

Finally, we emphasize that describing a two-dimensional free electron gas solely by a Drude response (second term in eqn (4)) with a single resonance frequency ω_p constitutes only a first-order approximation. A more refined

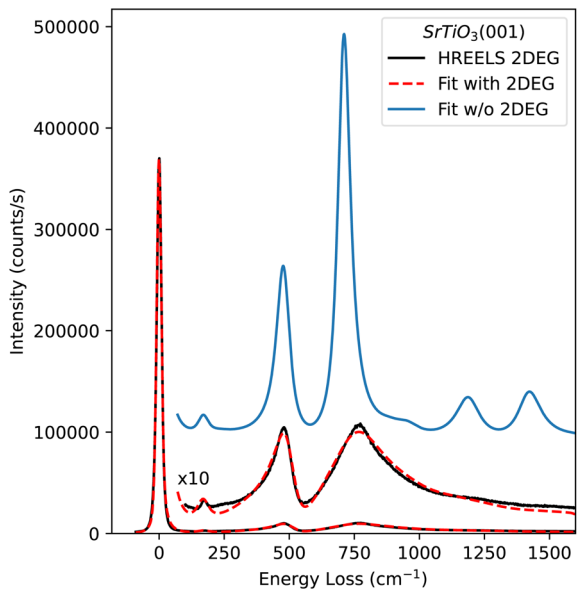

Fig. 9 HREELS spectrum of $SrTiO_3$(001) with 2DEG in a wider loss energy range: experimental data (black line) and fit by a generalized oscillator model including a Drude response (red dashed line) with plasma frequency $\omega_p = 950$ cm^{-1} and Drude damping constant $\gamma_p = 1100$ cm^{-1}. Fit without the Drude response (blue line; upshifted for clarity).

treatment should account for the presence of multiple electron bands with different effective masses, as well as potentially different spatial confinement (thicknesses), but also more complex responses as, *e.g.*, discussed for Si with a Cole–Davidson model might refine the description.[31] Nevertheless, the present study clearly demonstrates the strong coupling between surface phonon polaritons and free-carrier-induced surface plasmon polaritons, as well as the pronounced sensitivity of this interaction to the frequency-dependent properties of ultrathin electron gases at oxide surfaces.

Conclusions

The low-energy excitations of the $SrTiO_3$(001) surface have been analyzed based on high-resolution electron energy loss spectroscopy. Three dipole-active surface phonon polaritons have been identified and their line shapes have been analyzed in detail. The experimental HREELS spectra are well described by a generalized oscillator model that takes different damping of transverse optical (TO) and longitudinal optical (LO) modes into account. The corresponding bulk phonon frequencies and damping constants are in good agreement with previous reports based on bulk-sensitive techniques such as, *e.g.*, infrared spectroscopy of similarly doped samples.

Upon creation of a two-dimensional electron gas (2DEG) at the $SrTiO_3$(001) surface by annealing under ultrahigh-vacuum conditions, we observe pronounced asymmetric Fano-like line shapes of the surface phonon polaritons due to coupling with surface charge carriers in the 2DEG. The HREELS spectra can be well described by a dielectric response of the $SrTiO_3$(001) sample which includes an additional Drude response within a thin surface-near layer that is located on top of a $SrTiO_3$ sample without free charge carriers. The coupling between surface phonon polaritons and the free-carrier induced surface plasmon polariton leads to new hybrid modes with an avoided crossing behavior as a function of the plasma frequency of the Drude response. The strong coupling between lattice vibrations and free charge carriers results in substantial line broadening and asymmetric Fano-like line shapes of the surface phonon polaritons as observed experimentally. The interplay between the lattice vibrations and the electronic states at the surface is crucial for understanding the vibrational and electronic properties of oxide interfaces and their potential applications in oxide electronics.

Conflicts of interest

There are no conflicts to declare.

Data availability

The data is available *via* Zenodo at https://doi.org/10.5281/zenodo.17931973.

References

1 J. Goodenough, *Magnetism and the Chemical Bond*, Interscience Publishers (Wiley), New York, 1963, p. 394.
2 M. Imada, A. Fujimori and Y. Tokura, *Rev. Mod. Phys.*, 1998, **70**, 1039.

3 N. Spaldin and M. Fiebig, *Science*, 2005, **309**, 391.
4 J. Varignon, L. Vila, A. Barthélémy and M. Bibes, *Nat. Phys.*, 2018, **14**, 322.
5 A. Johansson, B. Göbel, J. Henk, M. Bibes and I. Mertig, *Phys. Rev. Res.*, 2021, **3**, 013275.
6 J. Devreese and A. Alexandrov, *Rep. Prog. Phys.*, 2009, **72**, 066501.
7 J. Last, *Phys. Rev.*, 1957, **105**, 1740.
8 J. Slater, *Phys. Rev.*, 1950, **78**, 748.
9 J. Axe, *Phys. Rev.*, 1967, **157**, 429.
10 K. Müller, W. Berlinger and E. Tosatti, *Z. Phys. B: Condens. Matter*, 1991, **84**, 277.
11 T. Kurosawa, *J. Phys. Soc. Jpn.*, 1961, **16**, 1298.
12 D. Berreman and F. Unterwald, *Phys. Rev.*, 1968, **174**, 791.
13 R. Lowndes, *Phys. Rev. B: Condens. Matter Mater. Phys.*, 1970, **1**, 2754.
14 F. Gervais and B. Piriou, *J. Phys. C: Solid State Phys.*, 1974, **7**, 2374.
15 A. Santander-Syro, O. Copie, T. Kondo, F. Fortuna, S. Pailhes, R. Weht, X. Qiu, F. Bertran, A. Nicolaou, A. Taleb-Ibrahimi, P. Le Fevre, G. Herranz, M. Bibes, N. Reyren, Y. Apertet, P. Lecoeur, A. Barthelemy and M. Rozenberg, *Nature*, 2011, **469**, 189.
16 P. King, S. McKeown Walker, A. Tamai, A. de la Torre, T. Eknapakul, P. Buaphet, S. Mo, W. Meevasana, M. Bahramy and F. Baumberger, *Nat. Commun.*, 2014, **5**, 3414.
17 D. Vaz, P. Noël, A. Johansson, B. Göbel, F. Bruno, G. Singh, S. McKeown-Walker, F. Trier, L. Vicente-Arche, A. Sander, S. Valencia, P. Bruneel, M. Vivek, M. Gabay, N. Bergeal, F. Baumberger, H. Okuno, A. Barthélémy, A. Fert, L. Vila, I. Mertig, J.-P. Attané and M. Bibes, *Nat. Mater.*, 2019, **18**, 1187.
18 P. Noël, F. Trier, L. Vicente Arche, J. Bréhin, D. Vaz, V. Garcia, S. Fusil, A. Barthélémy, L. Vila, M. Bibes and J.-P. Attané, *Nature*, 2020, **580**, 483.
19 H. Ibach, *J. Electron Spectrosc. Relat. Phenom.*, 1993, **64–65**, 819.
20 K. Kostov, S. Polzin and W. Widdra, *J. Phys.: Condens. Matter*, 2011, **23**, 484006.
21 K. Kostov, S. Polzin, S. Saha, O. Brovko, V. Stepanyuk and W. Widdra, *Phys. Rev. B: Condens. Matter Mater. Phys.*, 2013, **87**, 235416.
22 J. Premper, F. Schumann, A. Dhaka, S. Polzin, K. Kostov, V. Goian, D. Sander and W. Widdra, *Phys. Status Solidi B*, 2020, **257**, 1900650.
23 F. Wührl, A. Rieche, A. Oelschläger, K. Dörr and W. Widdra, *New J. Phys.*, 2026, **28**, 013501.
24 G. Koster, B. Kropman, G. Rijnders, D. Blank and H. Rogalla, *Appl. Phys. Lett.*, 1998, **73**, 2920.
25 P. Lambin, J.-P. Vigneron and A. Lucas, *Comput. Phys. Commun.*, 1990, **60**, 351.
26 F. Gervais, J.-L. Servoin, A. Baratoff, J. Bednorz and G. Binnig, *Phys. Rev. B*, 1993, **47**, 8187.
27 H. Raether, in *Surface Plasmons on Smooth Surfaces*, ed. H. Raether, Springer Berlin Heidelberg, Berlin, Heidelberg, 1988, p. 4.
28 G. Naik, V. Shalaev and A. Boltasseva, *Adv. Mater.*, 2013, **25**, 3264.
29 A. Santander-Syro, F. Fortuna, C. Bareille, T. Rödel, G. Landolt, N. Plumb, J. Dil and M. Radović, *Nat. Mater.*, 2014, **13**, 1085.
30 P. Lambin, J. Vigneron and A. Lucas, *Phys. Rev. B: Condens. Matter Mater. Phys.*, 1985, **32**, 8203.
31 R. Ulbricht, E. Hendry, J. Shan, T. Heinz and M. Bonn, *Rev. Mod. Phys.*, 2011, **83**, 543.